Biomedical Signal Processing and Control 62 (2020) 102073

Contents lists available at ScienceDirect

Biomedical Signal Processing and Control

journal homepage: www.elsevier.com/locate/bspc

Evaluating five different adaptive decomposition methods for EEG signal seizure detection and classification

Vinícius R. Carvalho [b,c], Márcio F.D. Moraes [a,c], Antônio P. Braga [b], Eduardo M.A.M. Mendes [a,b,c,*]

[a] Centro de Tecnologia e Pesquisa em Magneto-Ressonância, Escola de Engenharia, Universidade Federal de Minas Gerais, Av. Antônio Carlos, 6627, Pampulha, 31270 901, Belo Horizonte, Minas Gerais, Brazil
[b] Programa de Pós-Graduação em Engenharia Elétrica, Universidade Federal de Minas Gerais, Av. Antônio Carlos, 6627, Pampulha, 31270 901, Belo Horizonte, Minas Gerais, Brazil
[c] Núcleo de Neurociências, Departamento de Fisiologia e Biofísica, Instituto de Ciências Biológicas, Universidade Federal de Minas Gerais, Av. Antônio Carlos, 6627, Pampulha, 31270 901, Belo Horizonte, Minas Gerais, Brazil

ARTICLE INFO

Article history:
Received 16 December 2019
Received in revised form 15 April 2020
Accepted 5 July 2020
Available online 26 June 2020

ABSTRACT

Signal processing and machine learning methods are valuable tools in epilepsy research, potentially assisting in diagnosis, seizure detection, prediction and real-time event detection during long term monitoring. Recent approaches involve the decomposition of EEG signals into different modes in a data-dependent and adaptive way, which may provide advantages over commonly used Fourier based methods when dealing with nonlinear and non-stationary data. Examples of such methods include empirical mode decomposition (EMD), extended EMD (EEMD), complete EEMD with adaptive noise (CEEMDAN), empirical wavelet transform (EWT) and variational mode decomposition (VMD). In this work, feature sets extracted from original non-decomposed signals and from the aforementioned adaptive decomposition methods are evaluated for the classification of EEG seizure data using two freely available datasets. We provide a previously unavailable common methodology for comparing the performance of these methods for EEG seizure detection, with the use of the same classifiers, parameters and spectral and time domain features. Overall, results were similar between the evaluated decomposition methods, with slightly superior values for VMD and CEEMDAN. Features extracted from the original non-decomposed signals resulted in inferior class separability, but fairly accurate predictions could still be achieved with specific classifiers. The evaluated decomposition methods are promising approaches for seizure detection, but their use should be judiciously analysed, especially in situations that require real-time processing and computational power is an issue. Another contribution of this work is the development of python packages for EWT (ewtpy) and VMD (vmdpy), already available at the PyPI repository.

1. Introduction

Epilepsy is a burdening neurological disease that has a prevalence rate of around 6 per 1000 persons and incidence rate of 61 per 1000 person-years [1]. One of the factors contributing for its high incidence rate is the large number of causes leading to this condition, such as: genetic predisposition, dysplasia, cerebrovascular disease (CVD), trauma, tumor, infection, ischemia, among others [2].

Recurrent seizures are considered the hallmark of Epilepsy. These events reflect the abnormal firing of groups of neurons in the brain, in general synchronous and of high intensity [3]. This deviation from the normal functioning patterns of neurons may invoke sensations varying from strange feelings, behaviors and sensations to seizures with muscular spasms and possible loss of conscience [4].

The electroencephalogram (EEG) is a high temporal resolution recording of brain electrical activity and an essential method for the diagnosis of epilepsy and other neurological disorders. EEG can reflect abnormal neuronal activity during ictal (i.e. seizures) or interictal periods, such as sharp transients occurring in-between seizures [5]. These signals are commonly interpreted by experienced neurologists through visual inspection, taking into account features such as frequency, amplitude and regularity of waveforms,

* Corresponding author at: Departamento de Engenharia Eletrônica, Universidade Federal de Minas Gerais, Av. Antônio Carlos 6627, 31270-901, Belo Horizonte, MG, Brasil.
E-mail address: emmendes@cpdee.ufmg.br (E.M.A.M. Mendes).

https://doi.org/10.1016/j.bspc.2020.102073
1746-8094/

reactivity to stimuli, spatial range and temporal persistence of the signal's anomalies [6]. However, this method may be cumbersome and time consuming, especially for long series and multi-channel data, which can lead to an increasingly high ratio of false-negative results. Furthermore, there is a series of subtle signal features and components, as well as inter-channel relationships, which are virtually impossible to detect by simple visual inspection. This task may be assisted by signal processing and classification algorithms [7] that can deal with signal nonlinearities and subtleties, high-dimensional data and real-time processing. As such, these automated methods are valuable tools for the diagnosis, detection and prediction of epilepsy and epileptic seizures [8].

A variety of algorithms and signal processing techniques have been developed for the extraction of relevant features related to the epileptic phenomena [9]. Methods which analyze frequency components using the Fourier Transform are not always recommended, because EEG signals contain non-stationary components, violating conditions for the use of such transform [10]. Thus, recent methods for EEG analysis of epileptic patients may use time-frequency approaches, or non-linear methods such as Lyapunov exponents, fractal dimension, entropy or correlation dimension [11]. Other methods include the use of signal decomposition in adaptive ways, such as the Empirical Mode Decomposition (EMD), proposed by Huang et al. [10].

Of particular interest to the work presented here, the EMD is an adaptive and data-dependent decomposition method that successively extracts intrinsic mode functions (IMFs), defined by amplitude modulated (AM) and frequency modulated (FM) components. Accordingly, complex non-linear and non-stationary signals can be decomposed into a finite number of IMFs, each with well-behaved Hilbert transforms [10]. Extensions to the EMD method have been proposed to deal with multivariate data [12,13] and to alleviate the problem of mode mixing – when signal amplitudes of widely different scales are present within the same IMF or a signal with similar scale is divided into different IMF components [14,15]. Examples of the latter include ensemble empirical mode decomposition (EEMD) [15] and complete ensemble EMD with adaptive noise (CEEMDAN) [14]. The EMD and its extensions [16,17] have been successfully used in epilepsy research [16–21]. However, drawbacks such as computational cost, lack of theory (due to its algorithmic approach) and difficulty in interpreting the large number of modes have motivated the use and evaluation of different adaptive decomposition methods in seizure EEG signals [22].

The empirical wavelet transform (EWT) [22] addresses some limitations of EMD. By adapting some of the wavelet formalisms, this method designs appropriate wavelet filter banks and decomposes a signal into a predetermined number of modes. The use of EWT has been explored in different areas such as compression of electrocardiogram (ECG) signals [23], decomposition of seismic activity [24] and time-frequency representation of non-stationary signals [25]. Although the use of wavelets for seizure detection and classification has been widely explored [6,26–28], few works evaluate EWT for processing seizure EEG signals [29,30].

Another adaptive method denominated variational mode decomposition [31] (VMD) decomposes a signal into its principal modes adaptively and non-recursively. The method is related to the so-called Wiener filter, a property which grants it advantages in relation to noise robustness. Similar to what happened in the case of EWT, few works have evaluated VMD use for seizure EEG analysis [32–34].

When processing EEG from ictal phenomena, features generated from the use of the aforementioned decomposition methods are promising tools. In addition to their adaptive capabilities and ability to deal with nonlinear and non-stationary signals, extracted modes (or signal components) are compact around specific center frequencies and have well-behaved Hilbert transforms. This enables the extraction of features related to amplitude or bandwidth modulation, as well as instantaneous phase and amplitude. This work aims to compare different adaptive decomposition methods for EEG signal seizure detection using a freely available database and a common methodology, by extracting the same set of features and classifiers. So far this comparison has been hampered not only by the small number of works using EWT and VMD, but also by the fact that EMD, EEMD, CEEMDAN, VMD and EWT are evaluated in the seizure detection literature using different methodologies. In this work, results are also compared with features extracted from original non-decomposed signals. Expected results are performance improvements with the use of adaptive decomposition methods (EMD, EEMD, CEEMDAN, EWT and VMD), but similar overall performances among them.

The rest of this work is organized into three sections. In Section 2, the used methodology is presented, containing the used data, decomposition methods, description of extracted features and classification problem. In Section 3, the obtained results are presented for both datasets, followed by the discussion in Section 4. Concluding remarks are left for the last section.

2. Methods

2.1. Dataset

This work uses two public online EEG datasets: (i) one is offered by the University of Bonn [35] and is commonly used as benchmark for seizure detection algorithms and (ii) another from epilepsy patients collected at the Neurology and Sleep Centre, Hauz Khas, New Delhi (NSC-ND) [36].

2.1.1. University of Bonn (UoB) dataset

This dataset is divided into 5 subsets: *Z, O, N, F, S* (or A, B, C, D, E) [35]. Each subset contains 100 temporal series with a sampling frequency of 173.6 Hz and duration of 23.6 seconds. The Z and O classes correspond to surface EEG recordings of 5 healthy volunteers, with eyes open and closed, respectively. The rest of the subsets belong to presurgical recordings of epileptic patients. Set S contains seizure activity, while sets F and N are from seizure-free intervals, with electrodes placed on the epileptogenic zone and opposite hippocampus, respectively.

This work deals with a classification problem using three subsets: S, F and Z (E, D and A), corresponding to ictal, interictal and normal classes, respectively. Samples from each class and their regularized spectra, given by the Gaussian-filtered fast Fourier transform (FFT) of each signal are shown in Fig. 1. The first stage of processing of this dataset consists of applying a zero-phase 4th order lowpass Butterworth filter with cutoff frequency of 40 Hz [35].

2.1.2. Neurology and sleep centre - New Delhi (NSC-ND)

This dataset contains segmented EEG recordings acquired at the Neurology and Sleep Centre, Hauz Khas, New Delhi. Each signal was sampled at 200 Hz, band-pass filtered from 0.5 Hz to 70 Hz and segmented in windows of 5.12 s [37]. Each EEG segment was assigned one of three classes – pre-ictal, interictal and ictal (sets X, Y and Z, respectively). The used dataset consists of 150 segments (50 for each class) from one patient available at [38]. Fig. 2 shows EEG data and respective spectra from samples of each class from this dataset.

This work considers two classification problems for this dataset: (i) inter-ictal versus ictal (Y-Z) and (ii) all three classes (preictal, normal and ictal – X-Y-Z).

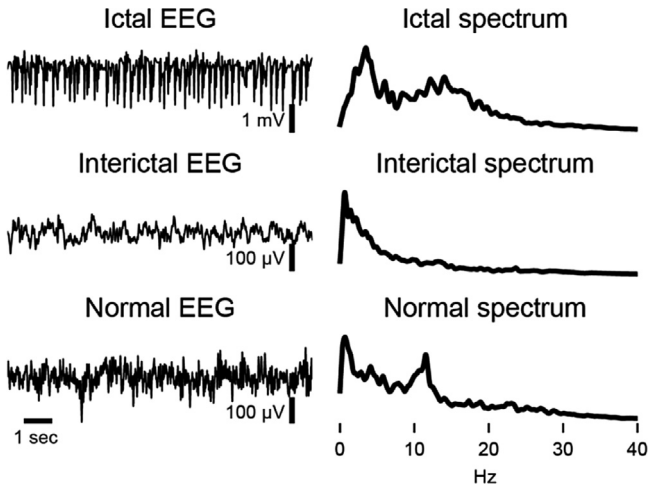

Fig. 1. Representative EEG data of the UoB dataset. EEG segments of each class (ictal, interictal and normal) and respective spectra.

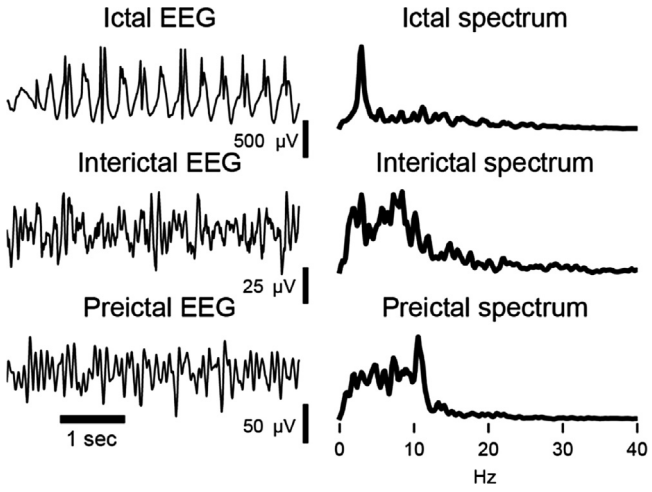

Fig. 2. Representative EEG signals of the NSC-ND dataset. EEG segments of each class (ictal, interictal and preictal) and respective spectra.

2.2. Analytical procedure and adaptive decomposition methods

An outline of the analytical procedure that follows is given in Fig. 3. In brief, signals are decomposed into N modes or IMFs, either by EMD, EEMD, CEEMDAN, EWT or VMD. This is followed by feature extraction of each mode and subsequent feature selection, defining a set of inputs to the selected classifiers. Next, performance metrics are calculated for each classifier, enabling the evaluation of each adaptive decomposition method for seizure detection and classification. Each processing step is summarized in the following sections.

2.2.1. Empirical mode decomposition (EMD)

The EMD is an interesting method due to its adaptability, not depending on assumptions such as linearity or stationarity. This method aims to divide the analyzed signal into a series of intrinsic mode functions (IMFs), where each IMF must satisfy to two relatively simple conditions:

I The number of extrema must be equal or differ by one (at most) in relation to the number of zero crossings.
II The mean envelope value, defined by the local maxima and minima, must be equal to zero.

The algorithm proposed by Huang et al. [10] for obtaining IMFs consists of a sifting process described by the following steps:

Given an input temporal series $f(t)$,

1) Find the local maxima and minima of the temporal series.
2) Generate the envelopes emax and emin by cubic spline interpolation of maxima and minima, respectively.
3) Calculate the mean of the envelopes: $m_i(t) = (e_{max}(t) + e_{min}(t))/2$
4) Subtract the value found previously from the signal: $h(t) = f(t) - m_i(t)$.
5) Check if the extracted signal $h(t)$ fulfills the two IMF conditions (zero mean and number of maxima and minima). IF this condition is satisfied, an IMF $c_i(t) = h(t)$ is found. ELSE, repeat steps 1-5 on the extracted signal.
6) A new residue r is generated: $r(t) = f(t) - c_i(t)$. Repeat steps 1 to 5, applied to the residue r, in order to find the remaining IMFs. The process halts when it is no longer possible to compute an IMF from a residue, which is then defined as a final residue r_M.

The signal is thus decomposed into a determined number of IMFs $c_i(t)$ in addition to residue r_M, as shown by (1),

$$f(t) = r_M + \sum_{i=1}^{N} c_i(t) \tag{1}$$

where N is the total number of IMFs found.

Unlike methods such as the discrete wavelet transform, which extracts low frequencies (or approximations) first and detail levels (corresponding to higher frequencies) later, the first IMFs isolated by EMD correspond to high frequencies of the signal and slower components are progressively extracted by the sifting process.

2.2.2. Ensemble empirical mode decomposition (EEMD)

EEMD is a noise-assisted data analysis (NADA) method, in which the resulting modes are obtained by averaging the results of decomposition over an ensemble of noisy versions of the original signal [15]. This aims to eliminate the mode mixing problem and preserve physical uniqueness of decomposition of signals of interest. Briefly, the method consists of the following steps:

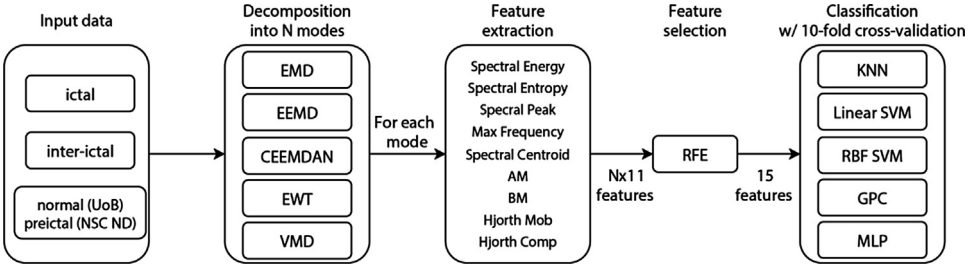

Fig. 3. Outline of the processing steps. EEG input data samples are decomposed into N modes with EMD, EEMD, CEEMDAN, EWT or VMD. After the extraction of 11 features from each mode, a feature selection method is applied to choose the relevant ones for classification. Different classifiers are trained and tested with a cross-validation method.

1) add white noise to the targeted input series
2) decompose the resulting signal plus noise from step 1 into IMFs
3) successively repeat step 1 and step 2 with different white noise signals
4) calculate the ensemble means of corresponding IMFs of the decompositions as the final result

Although this method solves the mode mixing problem, the EEMD has drawbacks such as residual noise being present in the reconstructed EEMD signal and different realizations of the same input data producing a different number of modes. In order to overcome these problems, the CEEMDAN method was proposed [14].

2.2.3. Complete ensemble empirical mode decomposition with adaptive noise (CEEMDAN)

This work implements the improved version of CEEMDAN [39]. Let $w^{(i)}$ be a realization of Gaussian white noise with zero mean and unit variance, $\sim IMF_k$ the extracted decomposition modes and $E_k(\cdot)$ the operator that results in the k-th mode of a signal decomposed by EMD and $M(\cdot)$ the operator producing the mean of a signal. Given an input temporal series $f(t)$, the algorithm is described as follows:

1) decompose with EMD I realizations of noise-added signals $f^i(t) = f(t) + \beta_0 E_1(w^i)$. Compute the first residue $r_1(t) = \left\langle M(f^i(t)) \right\rangle$. $\beta_k = \varepsilon_k std(r_k)$
2) calculate the first mode $\sim IMF_1(t) = f(t) - r_1(t)$.
3) get second residue by averaging local means of realizations $r_1(t) + \beta_1 E_2(w^i)$, obtaining the second mode as $\sim IMF_2(t) = r_1(t) - r_2(t) = r_1(t) - \left\langle M(r_1(t) + \beta_1 E_2(w^i)) \right\rangle$.
4) calculate the k-th residue: $r_k(t) = \left\langle M(r_{k-1}(t) + \beta_{k-1} E_k(w^i)) \right\rangle$ for $k = 3, \ldots, K$.
5) calculate the k-th mode: $\sim IMF_k(t) = r_{k-1}(t) - r_k(t)$
6) go back to step 4 for the next k. Repeat until residues cannot be further decomposed (residue has a maximum of one extreme at most)

The improved CEEMDAN method offers major improvements in relation to EMD and EEMD, such as avoiding spurious modes and reducing noise contamination, which confers more physical meaning to extracted IMFs

This work used the pyEMD Python package [40] for the implementation of EMD, EEMD and CEEMDAN.

2.2.4. Empirical wavelet transform (EWT)

As in EMD, the EWT method aims to extract the oscillatory amplitude (AM) and frequency (FM) components of a signal, considering these as having compact Fourier support. It addresses some limitations of EMD, such as the lack of mathematical theory. Unlike traditional wavelet transforms, which use predefined filter bank structures, the EWT method defines the supports of the filters in accordance with the spectral distribution of the signal, in a fully adaptive way. Some considerations are made for analysis: (1) the signal must be real valued, due to the need for symmetry, and (2) a normalized frequency axis with 2π periodicity is considered, but analysis is restricted to $[0, \pi]$, due to Shannon's sampling criterion.

A summary of the EWT method is given next, followed by a more detailed description.

1) define a number N of empirical modes
2) computes signal spectrum
3) find N-1 local spectral maxima
4) set boundaries ωn - midpoints between two consecutive maxima

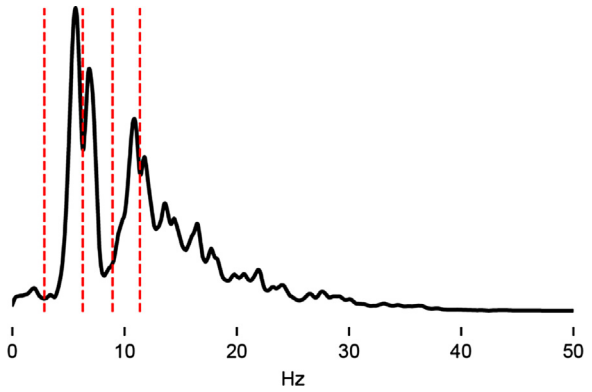

Fig. 4. Spectral segmentation of ictal EEG (UoB dataset) into 5 modes. For the EWT method, boundaries are defined as midpoints between two consecutive local spectrum maxima.

5) according to the limits ωn, define EWT filter bank
6) apply to input signal to obtain N empirical modes

A number of modes N is defined a priori, determining how the original signal will be decomposed and how many segments the spectrum is partitioned in the range $[0, \pi]$. Among the N + 1 frequency boundaries to be determined, two are already predefined (ω_0 and ω_N), corresponding to frequencies of 0 and π, respectively.

The remaining N-1 limits are set according to the distribution of the signal's frequency spectrum: the N-1 local maxima are found, and the boundaries ω_n (n = 1, 2, ... N-1) are defined as midpoints between two consecutive maxima. In this work, maxima were detected on the smoothed spectrum that is obtained by applying a Gaussian filter (filter length = 25, σ = 5 for UoB, 5 and 1 for NSC-ND) on the fast Fourier transform of each signal. The segmentation of a signal spectrum into 5 Modes is given in Fig. 4.

With limits ω_n defined, the segments $\Lambda_n = [\omega_{n-1}, \omega_n]$ fill the interval $[0, \pi]$. The limits of each segment are characterized by a transition period centered at the respective ω_n, with width equal to $2\tau_n$. Each segment is associated to a filter (lowpass for the ω_0, bandpass for the rest), the construction of which is related to Littlewood-Paley and Meyer wavelets [41]. Thus, an empirical scale function $\phi_n(\omega)$ and an empirical wavelet $\psi_n(\omega)$ are defined, corresponding to the approximation (low frequencies) and detail (higher frequencies) coefficients. These are constructed in such a way that a tight frame is obtained. Further details on the construction of such functions are given in Ref. [22].

With the conditions for building a tight frame satisfied, the EWT is defined similarly as the traditional wavelet transform, with details given by the inner product of the wavelet function with the signal, and the approximation equal to the inner product of the signal with the scaling function.

Based on Jérôme Gilles' MATLAB toolbox [42], a Python package of EWT (ewtpy) was developed for this work and is available at https://pypi.org/project/ewtpy/ and at https://github.com/vrcarva/ewtpy.

2.2.5. Variational mode decomposition (VMD)

The VMD method overcomes EMD's limitations such as lack of mathematical theory, as well as EWT's relatively strict filter bank boundaries. By adaptively determining the relevant bands with concurrent estimates of corresponding modes, errors are properly balanced between them. In addition, the method is robust to sampling and noise. When compared to EMD, VMD performed better in tests dealing with tone detection and separation [31].

In the variational mode decomposition, a predefined number K of modes are extracted by means of a constrained variational

optimization problem, solved using alternate direction method of multipliers (ADMM) [43,44]. Initially, the method assumes each mode k as having compact bandwidth in the Fourier spectrum, with a respective central frequency ω_k. The problem can be briefly described by the following scheme.

1) construction of a single-side band analytic signal from the real signal's Hilbert transform.
2) complex harmonic mixing – shift the frequency spectrum of each mode to baseband by multiplying it with an exponential function tuned to the estimated center frequency of the respective mode.
3) assess the bandwidth by the H^1-norm Gaussian smoothness of the demodulated signal – i.e. the squared L^2-norm of the gradient.

The resulting constrained variational problem is the given by:

$$min\left\{u_k\right\},\left\{\omega_k\right\}$$

$$\left\{\sum_k\left\|\partial_t\left[\left(\delta(t)+\frac{j}{\pi t}\right)*u_k(t)\right]e^{-j\omega_k t}\right\|_2^2\right\}\ s.t.\ \sum_k u_k=f \tag{2}$$

u_k is the kth mode of the signal (from 1 to K) and ω_k the respective center frequency. $\left\{u_k\right\}$ and $\left\{\omega_k\right\}$ represent the full set of modes and center frequencies, respectively. The input signal to be decomposed is given by f and δ is the Dirac function.

Equation (2) can be rendered as an unconstrained problem by introducing a quadratic penalty term and Lagrangian multipliers. The augmented Lagrangian is given by:

$$\mathcal{L}\left(\left\{u_k\right\},\left\{\omega_k\right\},\lambda\right):=\alpha\sum_k\left\|\partial_t\left[\left(\delta(t)+\frac{j}{\pi t}\right)*u_k(t)\right]e^{-j\omega_k t}\right\|_2^2$$

$$+\left\|f(t)-\sum_k u_k(t)\right\|_2^2+\left\langle\lambda(t),f(t)-\sum_k u_k(t)..\right\rangle \tag{3}$$

Solving Eq. (3) with ADMM yields all the K estimated modes in the frequency domain ($\hat{u}_k$), for each iteration n:

$$\hat{u}_k^{n+1}(\omega)=\frac{\hat{f}(\omega)-\sum_{i<k}\hat{u}_i^{n+1}(\omega)-\sum_{i>k}\hat{u}_i^{n}(\omega)+\frac{\hat{\lambda}^n(\omega)}{2}}{1+2\alpha(\omega-\omega_k^n)^2} \tag{4}$$

It can be seen by Equation 4 that modes are updated by simple Wiener filtering. The center frequencies can be calculated as the corresponding center of gravity of the spectrum of each mode:

$$\omega_k^{n+1}=\frac{\int_0^\infty\omega\left|\hat{u}_k(\omega)\right|^2d\omega}{\int_0^\infty\left|\hat{u}_k(\omega)\right|^2d\omega} \tag{5}$$

The resulting modes in the time domain (u_k), represent the full decomposition of the original signal $f(t)$. For more detailed description of the method, the complete constrained variational optimization problem is available in Ref. [31].

Although the use of VMD for long-time EEG signals suffers from caveats due to non-stationarity, its use in this work is motivated by the relatively short duration of the time series from the used database, and the focus on classification rather than exact mode decomposition and reconstruction.

A Python package, based on the original MATLAB toolbox [45], was developed for this work and made available at https://pypi.org/project/vmdpy/ and at https://github.com/vrcarva/vmdpy. Both *ewtpy* and *vmdpy* can be readily installed with pip (*pip install vmdpy* and *pip install ewtpy*).

2.3. Hilbert Transform and Analytic signal

The presented decomposition methods have the interesting property of yielding modes/IMFs with "well-behaved" Hilbert transforms [10,31], from which features as instantaneous phase, frequency or envelope can be extracted. The analytic signal of each mode/IMF is given by Eq. (6).

$$z(t)=f(t)+jf_h(t)=A(t)e^{j\varphi(t)} \tag{6}$$

where $f_h(t)$ is the Hilbert transform of $f(t)$,

$$f_h(t)=f(t)*\frac{1}{\pi t}, \tag{7}$$

and $*$ is the convolution operator. Instantaneous amplitude and phase are defined as:

$$A(t)=\sqrt{f^2(t)+{f_h}^2(t)} \tag{8}$$

$$\varphi(t)=\arctan\left(\frac{f(t)}{f_h(t)}\right) \tag{9}$$

The instantaneous frequency of a given IMF can be calculated from its analytic signal with:

$$\omega(t)=\frac{d\varphi(t)}{dt} \tag{10}$$

By dividing a signal into a given number of modes/IMFs, features related to their respective analytic signals and spectra can be extracted.

2.4. Feature extraction

Modes given by the five aforementioned methods (EMD, EEMD, CEEMDAN, EWT and VMD) may be considered as amplitude and frequency modulated signals. Thus, feature extraction is made according to properties of the spectrum of each mode, with a similar approach used by Refs. [46] and [19].

The first feature extracted is the spectral power (SPow), given by Eq. (11).

$$Spow=\frac{1}{N}\sum_{f=0}^{\frac{f_s}{2}}P_{XX}(f), \tag{11}$$

where N is the total number of spectral coefficients, and P_{XX} is the mode PSD estimated by Welch's method [47]. The second feature is the Spectral entropy (SEnt), shown in Eq. (12).

$$SEnt=-\sum_{f=0}^{\frac{f_s}{2}}\overline{P}_{XX}(f)\log\left[\overline{P}_{XX}(f)\right] \tag{12}$$

$\overline{P}_{XX}$ is the normalized PSD. The following three features are related by the main frequency component of the respective mode. After determining the global maximum of P_{XX}, the corresponding magnitude is defined as the spectral peak (SP), as well as the associated frequency (f), defining the 3rd and 4th features. The following feature is the spectral centroid (SC) of the respective mode, defined in Eq. (13):

$$SC=\frac{\sum_{f=0}^{\frac{f_s}{2}}\omega(f)M(f)}{\sum_{f=0}^{\frac{f_s}{2}}M(f)}, \tag{13}$$

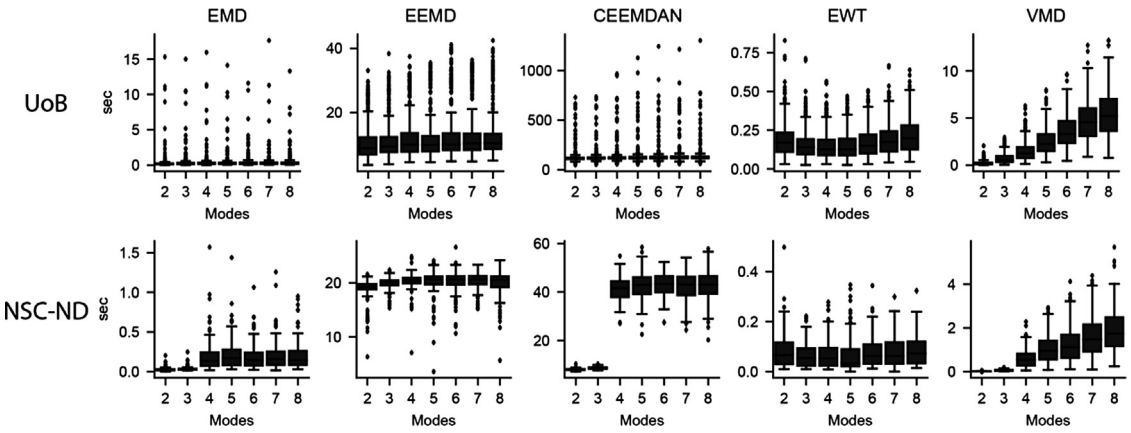

Fig. 5. Execution times for each adaptive decomposition algorithm. EWT shows the lowest computational cost, followed by EMD, VMD and extended versions of EMD.

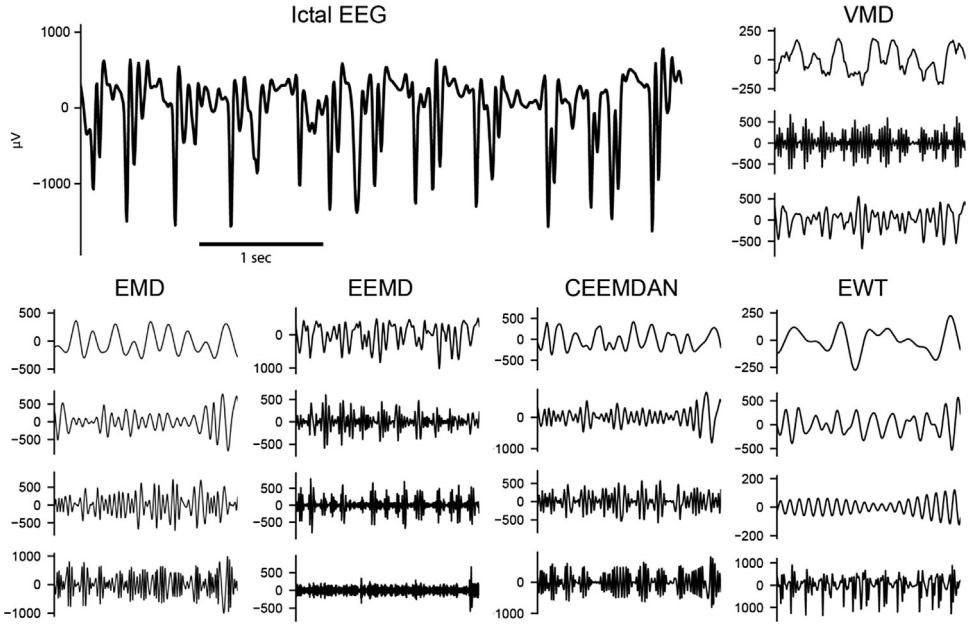

Fig. 6. Decomposition of ictal EEG from the UoB dataset. Short segment of raw EEG segments and the resulting IMFs/modes from EMD, EEMD, CEEMDAN (bottom subplots show residues), EWT and VMD.

where f is the frequency bin, and $\omega(f)$ and $M(f)$ are respectively, the central frequency and magnitude of the PSD of bin f. The last two spectral features are the AM and FM bandwidths, defined by Eqs. (14) and (15) [48]:

$$B^2{}_{AM} = \frac{1}{E}\int \left(\frac{dA(t)}{dt}\right)^2 dt \tag{14}$$

$$B^2{}_{FM} = \frac{1}{E}\int \left(\frac{d\phi(t)}{dt} - \langle\omega\rangle\right)^2 A^2(t)\,dt, \tag{15}$$

where A is the amplitude of the analytic signal, E is the Energy and $\langle\omega\rangle$ is the center frequency of the current mode, given by Eq. (16).

$$\langle\omega\rangle = \frac{1}{E}\int \frac{d\phi(t)}{dt} A^2(t) dt \tag{16}$$

Time-domain features are also extracted from each mode: Hjorth parameters [49] and statistical moments.

Hjorth mobility (*Mob*) is related to the mean frequency of the signal and proportional to the variance of its spectrum, while Hjorth complexity (*Comp*) is an estimate of the signals' bandwidth [50]. These are defined by:

$$Mob(x) = \sqrt{\frac{Var\left(\frac{dx(t)}{dt}\right)}{Var(x(t))}} \tag{17}$$

$$Comp(x) = \frac{Mob\left(\frac{dx(t)}{dt}\right)}{Mob(x(t))}, \tag{18}$$

where $f(t)$ is the current signal component, and Var() is the variance.

The skewness is related to the signal distribution's asymmetry, and is given by the following equation:

$$S(x) = E\left[\left(\frac{x(t)-\mu}{\sigma}\right)^3\right] \tag{19}$$

The standard deviation of $f(t)$ is represented by σ, and its mean by μ. The kurtosis is related to the tails of the distribution yielded by the signal and is given by.

$$S(x) = E\left[\left(\frac{x(t)-\mu}{\sigma}\right)^4\right] \quad (20)$$

2.5. Feature selection and classification

For feature selection and classification algorithms, functions from scikit-learn package [51] were used.

Since the number of extracted features of each signal is relatively large, and not every feature is relevant for class discrimination, there is a need for a feature selection or ranking method. In this work, this selection was done with recursive feature elimination (RFE) [52] applied to the radial basis function (RBF) support vector machine (SVM) classifier. Afterwards, different classification methods were evaluated: (I) k-nearest neighbors (KNN) [53] with three neighbors, uniform weights and Euclidean distance metric, (II) linear (penalty parameter C = 0.025,) and RBF (C = 1.0) SVM [54] with *gamma* = 'scale' and tolerance for stopping criteria = 0.001, (III) Gaussian process classification (GPC) based on Laplace approximation [55] with RBF kernel and (IV) a multi-layer perceptron (MLP) [56] with 1 hidden layer with 100 neurons, rectified linear unit activation function (*relu*), "*adam*" solver, *alpha* (regularization term) = 0.0001 and constant learning rate (0.001).

The classification problem involves three classes for the UoB dataset (normal, interictal and ictal, 100 samples each) and two or three classes for the NSC-ND dataset; (i) interictal and ictal or (ii) pre-ictal, interictal and ictal. In order to verify the classification algorithms' performance, 10-fold cross-validation was used. For performance evaluation, four common measures were employed; accuracy (ACC), specificity (SPEC), sensitivity (SEN) and area under the receiver operating characteristic (ROC) curve (AUC). The last three measures are calculated by binarizing classifier output labels, choosing the ictal class as positive. Finally, classification training times of each fold are measured.

3. Results

Algorithms were implemented in Python 3.7 on a workstation with an Intel Core i7-8700 K CPU and 64 GB RAM. All scripts used in this work are available online at https://github.com/vrcarva/carvalho-etal-2019.

Fig. 5 shows execution times for decomposing a single EEG signal from each dataset with different methods. Aside from VMD and CEEMDAN, increasing the maximum number of modes does not significantly affect the execution times, which vary considerably between methods. EWT is the fastest one, followed by VMD and EMD. Despite being described as having reduced computational cost in relation to EEMD, CEEMDAN resulted in higher execution times. This may be due to specific implementation details of the pyEMD package.

3.1. UoB dataset

Fig 6 illustrates the decomposition of a seizure EEG by EMD, EEMD, CEEMDAN, EWT and VMD. Figs. S1 and S2 show this for inter-ictal and normal signals, respectively.

Samples of each class were decomposed into N (2 to 8) modes, followed by the extraction of the 11 features from each one. Thus, each sample results in $N \times 11$ features for EWT/VMD and $(N+1) \times 11$ for EMD/EEMD/CEEMDAN (+1 since features are also extracted from residuals), from which the SVM-RFE algorithm selected a subset. Based on the accuracy values as a function of the number of features, as shown in S5 Fig., 20 features were selected for each classifier. RFE was not applied for the "control" (the raw, non-decomposed signal), which results in only 11 features for each sample. Afterwards, different classifiers are trained and tested, resulting in performance evaluation metrics. Ten iterations of training/testing were run, resulting in mean ± standard deviation for each performance parameter.

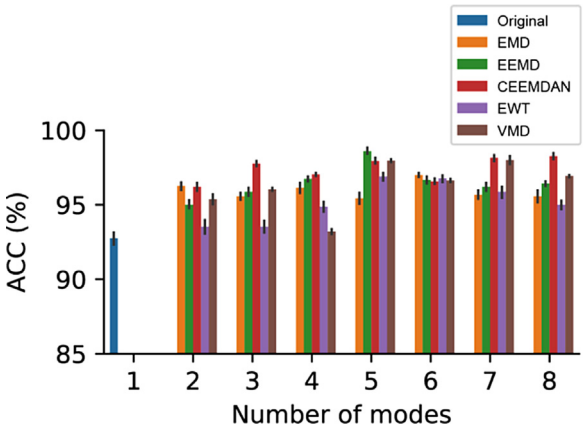

Fig. 7. Accuracy values as a function of decomposed modes. Using the RBF-SVM classifier, accuracy values are shown for features extracted from the original signal and from the analysed decomposition methods, varying the number of modes (or IMFs).

Fig. 7 shows the effect of varying the maximum number of modes on classification accuracy for each decomposition method. Although the maximum number of modes impacts performance, in none of the cases were accuracy values inferior to the ones obtained with features extracted from the original non-decomposed signal. Furthermore, the optimal number of modes is not the same for every method.

The best results for each classifier applied to each decomposition method (2 modes for EMD, 5 for EEMD, 5 for CEEMDAN, 5 for EWT and 7 for VMD) are detailed in Table 1 – measures of ACC, SEN, SPEC, AUC and execution times for each classification algorithm.

Minimum and maximum accuracies for each method are [94.5 97.7] % for EMD, [95.6 98.6] % for EEMD, [96.2 98.5] % for CEEMDAN, [92.8 97.1] % for EWT, [97.37 98.3] % VMD. Features from the original non-decomposed signal can also yield fairly accurate predictions (maximum of 95.1 % with GPC) but in general resulted in poor performance (minimum 89.7 % ACC).

3.2. NSC-ND dataset

Fig. 8 shows the decomposition of a seizure EEG from the NSC-ND dataset.

For both classification problems (X-Y-Z and Y-Z), only a subset of the 20 (40 for the GCP classifier) most relevant features was selected according to the RFE method. Fig. 9 shows the accuracy values for the RBF-SVM classifier for each decomposition method, varying the number of modes.

For most decomposition methods, varying the number of extracted modes has a significant impact on performance for most methods. Interestingly, the optimal number of modes is not the same for every method – while few IMFs yield better accuracy for EMD and CEEMDAN, more modes are needed for good performance in VMD. In the latter, this comes at the cost of increased execution times for extracting IMFs, as seen in Fig. 5. Choosing the optimal number of modes for each decomposition method, performance is detailed in Table 2 for the Y-Z classification problem. S6 Table shows detailed performance measures for the X-Y-Z case.

Table 1
UoB dataset (S-F-Z) classification performance (mean ± standard deviation) using different decomposition and classification methods.

Method	Modes	Measure	KNN	Linear SVM	RBF SVM	GPC	MLP
EMD	**2**	ACC (%)	95.13 ± 0.34	94.50 ± 0.40	96.27 ± 0.39	97.70 ± 0.38	97.13 ± 0.37
		SEN (%)	89.70 ± 0.64	93.20 ± 0.87	93.50 ± 1.02	96.40 ± 1.02	96.50 ± 0.81
		SPEC (%)	97.85 ± 0.59	95.15 ± 0.39	97.65 ± 0.23	98.35 ± 0.39	97.65 ± 0.50
		AUC × 100	97.76 ± 0.33	98.87 ± 0.29	99.69 ± 0.10	99.72 ± 0.02	99.73 ± 0.16
		Time (s)	0.30 ± 0.01	0.43 ± 0.03	0.73 ± 0.03	65.05 ± 4.15	27.54 ± 0.64
EEMD	**5**	ACC (%)	97.17 ± 0.48	95.63 ± 0.38	98.60 ± 0.33	97.03 ± 0.18	96.77 ± 0.26
		SEN (%)	94.40 ± 0.92	96.50 ± 0.81	96.00 ± 0.89	95.10 ± 0.54	94.20 ± 0.75
		SPEC (%)	98.55 ± 0.35	95.20 ± 0.33	99.90 ± 0.20	98.00 ± 0.22	98.05 ± 0.15
		AUC × 100	99.19 ± 0.17	99.40 ± 0.19	99.82 ± 0.08	99.74 ± 0.16	99.68 ± 0.13
		Time (s)	0.28 ± 0.02	0.41 ± 0.02	0.74 ± 0.03	57.65 ± 1.14	27.27 ± 1.07
CEEMDAN	**5**	ACC (%)	96.20 ± 0.22	97.07 ± 0.29	97.93 ± 0.33	98.03 ± 0.31	98.50 ± 0.40
		SEN (%)	91.10 ± 0.70	94.10 ± 0.70	95.90 ± 0.70	97.80 ± 0.87	97.80 ± 1.08
		SPEC (%)	99.25 ± 0.25	99.05 ± 0.42	99.45 ± 0.27	98.25 ± 0.40	99.35 ± 0.32
		AUC × 100	98.73 ± 0.31	99.14 ± 0.15	99.44 ± 0.09	99.57 ± 0.11	99.34 ± 0.13
		Time (s)	0.29 ± 0.02	0.46 ± 0.03	0.67 ± 0.04	58.43 ± 1.64	27.69 ± 1.09
EWT	**5**	ACC (%)	92.77 ± 0.72	94.87 ± 0.58	96.90 ± 0.40	95.30 ± 0.38	97.10 ± 0.40
		SEN (%)	88.40 ± 0.92	94.00 ± 1.00	96.70 ± 0.64	93.90 ± 1.04	95.90 ± 0.70
		SPEC (%)	95.05 ± 0.61	95.30 ± 0.56	97.10 ± 0.37	96.30 ± 0.60	97.70 ± 0.33
		AUC × 100	97.40 ± 0.43	99.21 ± 0.15	99.55 ± 0.12	99.36 ± 0.24	99.54 ± 0.12
		Time (s)	0.29 ± 0.02	0.42 ± 0.02	0.76 ± 0.04	55.44 ± 0.73	27.43 ± 0.57
VMD	**7**	ACC (%)	97.37 ± 0.18	97.77 ± 0.21	98.00 ± 0.45	98.33 ± 0.21	97.83 ± 0.27
		SEN (%)	94.70 ± 1.10	97.40 ± 0.66	98.80 ± 0.87	97.90 ± 0.54	96.40 ± 0.66
		SPEC (%)	98.75 ± 0.46	97.95 ± 0.15	97.60 ± 0.37	98.55 ± 0.27	98.55 ± 0.15
		AUC × 100	99.17 ± 0.10	99.56 ± 0.10	99.69 ± 0.10	99.68 ± 0.10	99.74 ± 0.10
		Time (s)	0.29 ± 0.02	0.39 ± 0.03	0.70 ± 0.04	68.85 ± 3.44	27.50 ± 1.09
-	**1**	ACC (%)	92.70 ± 0.55	89.73 ± 0.44	92.77 ± 0.67	95.10 ± 0.47	93.17 ± 0.40
		SEN (%)	89.70 ± 1.19	88.50 ± 0.67	89.10 ± 1.81	93.00 ± 1.41	90.00 ± 0.63
		SPEC (%)	95.80 ± 0.40	90.85 ± 0.67	95.20 ± 0.46	96.15 ± 0.67	95.20 ± 0.40
		AUC × 100	97.24 ± 0.37	97.10 ± 0.29	98.36 ± 0.31	98.45 ± 0.39	98.12 ± 0.25
		Time (s)	0.25 ± 0.03	0.38 ± 0.04	0.61 ± 0.05	61.00 ± 2.40	26.78 ± 1.32

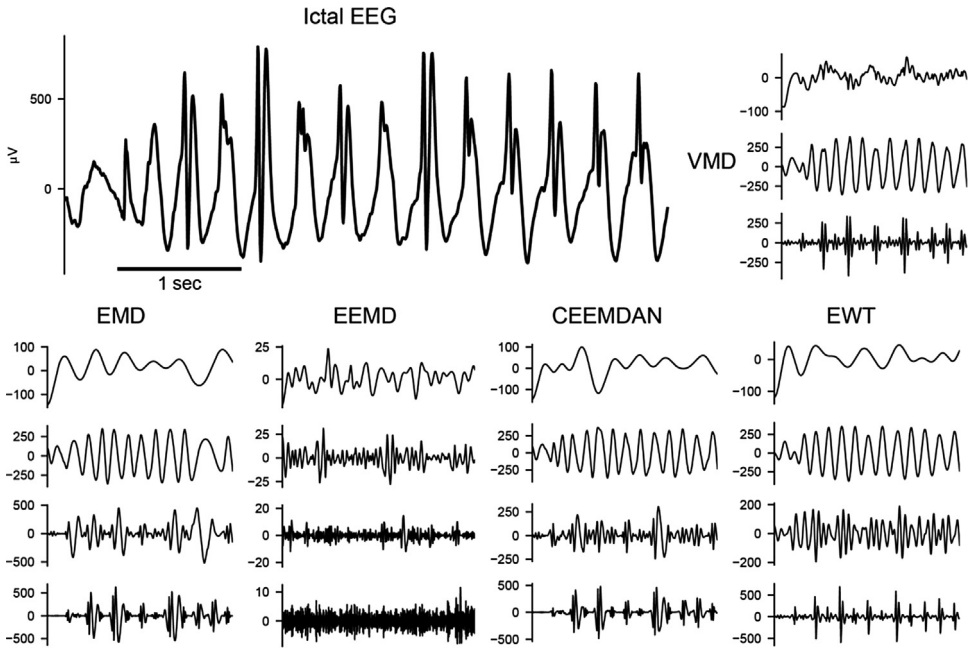

Fig. 8. Decomposition of ictal EEG from the NSC-ND dataset. Raw ictal EEG segment and resulting IMFs/modes from EMD, EEMD, CEEMDAN (bottom subplots show residues), EWT and VMD.

From Table 2, the Y-Z classification results in minimum and maximum accuracies for each method of: [97.2 99.0] % for EMD, [99.2 100] % for EEMD, [96.1 98.4] % for CEEMDAN, [98.8 100] % for EWT, [99.9 100] % VMD and [92.9 98.1] % for the original non-decomposed signal. From Sup. Table 1, the X-Y-Z classification results in minimum and maximum accuracies for each method of: [82.2 90.4] % for EMD, [79.9 85.3] % for EEMD, [78.5 93.1] % for CEEMDAN, [78.2 91.3] % for EWT, [88.3 92.1] % for VMD and [71.3 86.7] % for the original non-decomposed signal. Once again, good results with features from the raw signal depended on using a specific classifier (GPC) and decomposition methods provided overall good performances, with superior values for VMD.

A summarized comparison between results of the present work and a selection of few papers in the extensive literature of seizure detection is shown in Table 3.

Table 2
NSC-ND dataset, normal × ictal (Y-Z) classification performance (mean ± standard deviation) using different decomposition and classification methods.

Method	Modes	Measure	KNN	Linear SVM	RBF SVM	GPC	MLP
EMD	**2**	ACC (%)	97.20 ± 0.40	98.80 ± 0.40	99.00 ± 0.77	98.90 ± 0.54	98.60 ± 0.49
		SEN (%)	94.60 ± 0.92	97.80 ± 0.60	98.00 ± 1.55	98.20 ± 0.60	97.20 ± 0.98
		SPEC (%)	99.80 ± 0.60	99.80 ± 0.60	100.00 ± 0.00	99.60 ± 0.80	100.00 ± 0.00
		AUC×100	99.58 ± 0.37	99.92 ± 0.16	99.96 ± 0.12	99.96 ± 0.12	99.92 ± 0.16
		Time (s)	0.15 ± 0.01	0.10 ± 0.01	0.15 ± 0.02	3.91 ± 0.22	11.46 ± 0.19
EEMD	**3**	ACC (%)	100.00 ± 0.00	100.00 ± 0.00	99.20 ± 0.40	100.00 ± 0.00	100.00 ± 0.00
		SEN (%)	100.00 ± 0.00	100.00 ± 0.00	100.00 ± 0.00	100.00 ± 0.00	100.00 ± 0.00
		SPEC (%)	100.00 ± 0.00	100.00 ± 0.00	98.40 ± 0.80	100.00 ± 0.00	100.00 ± 0.00
		AUC×100	100.00 ± 0.00	100.00 ± 0.00	100.00 ± 0.00	100.00 ± 0.00	100.00 ± 0.00
		Time (s)	0.15 ± 0.01	0.09 ± 0.01	0.15 ± 0.01	4.71 ± 0.19	11.46 ± 0.40
CEEMDAN	**7**	ACC (%)	96.10 ± 0.54	98.00 ± 0.00	98.40 ± 0.49	97.20 ± 0.40	97.60 ± 0.49
		SEN (%)	95.60 ± 0.80	96.00 ± 0.00	96.80 ± 0.98	94.40 ± 0.80	95.20 ± 0.98
		SPEC (%)	96.60 ± 0.92	100.00 ± 0.00	100.00 ± 0.00	100.00 ± 0.00	100.00 ± 0.00
		AUC×100	98.80 ± 0.18	99.84 ± 0.20	99.96 ± 0.12	99.96 ± 0.12	99.96 ± 0.12
		Time (s)	0.14 ± 0.02	0.10 ± 0.01	0.14 ± 0.01	4.64 ± 0.18	11.54 ± 0.37
EWT	**3**	ACC (%)	100.00 ± 0.00	99.00 ± 0.00	98.80 ± 0.40	99.00 ± 0.00	99.00 ± 0.00
		SEN (%)	100.00 ± 0.00	100.00 ± 0.00	100.00 ± 0.00	100.00 ± 0.00	100.00 ± 0.00
		SPEC (%)	100.00 ± 0.00	98.00 ± 0.00	97.60 ± 0.80	98.00 ± 0.00	98.00 ± 0.00
		AUC×100	100.00 ± 0.00	99.68 ± 0.24	100.00 ± 0.00	100.00 ± 0.00	99.92 ± 0.24
		Time (s)	0.15 ± 0.01	0.09 ± 0.01	0.14 ± 0.01	4.76 ± 0.37	11.41 ± 0.29
VMD	**8**	ACC (%)	99.90 ± 0.30	99.90 ± 0.30	100.00 ± 0.00	100.00 ± 0.00	100.00 ± 0.00
		SEN (%)	99.80 ± 0.60	100.00 ± 0.00	100.00 ± 0.00	100.00 ± 0.00	100.00 ± 0.00
		SPEC (%)	100.00 ± 0.00	99.80 ± 0.60	100.00 ± 0.00	100.00 ± 0.00	100.00 ± 0.00
		AUC×100	99.98 ± 0.06	100.00 ± 0.00	100.00 ± 0.00	100.00 ± 0.00	100.00 ± 0.00
		Time (s)	0.15 ± 0.01	0.11 ± 0.01	0.15 ± 0.02	4.97 ± 0.25	11.36 ± 0.44
-	**1**	ACC (%)	92.90 ± 0.30	94.90 ± 0.30	93.30 ± 0.90	98.10 ± 0.54	96.50 ± 0.50
		SEN (%)	92.00 ± 0.00	94.00 ± 0.00	94.00 ± 1.79	96.60 ± 0.92	95.60 ± 0.80
		SPEC (%)	93.80 ± 0.60	95.80 ± 0.60	92.60 ± 0.92	99.60 ± 0.80	97.40 ± 0.92
		AUC×100	97.38 ± 0.42	96.40 ± 0.44	99.24 ± 0.22	99.96 ± 0.12	99.16 ± 0.85
		Time (s)	0.15 ± 0.01	0.09 ± 0.01	0.12 ± 0.01	4.65 ± 0.25	11.14 ± 0.45

Table 3
Comparison of results of the present work and selected state-of-the art of seizure detection algorithms using the UoB and NSC-ND datasets.

Dataset	Classes	Authors	Method	ACC (%)	SEN (%)	SPEC (%)
University of Bonn	ZO-FN-S	Sharma et al. [57]	higher-order statistics + DNN	99.6	100	99.3
	F-S	Zhang et al. [33]	VMD + quadratic feature extraction	97.4	97.1	96.7
		Gupta et al. [58]	DCT + Hurst Exponent + ARMA Parameters	96.5	96.4	96.2
	Z-S	Subasi et al. [59]	Hybrid SVM, GA/PSO	99.4	99.5	99.3
	O-F-S	Acharya et al. [60]	CNN	88.7	95.0	90.0
		Acharya et al. [61]	WPD + PCA + GMM	99	99	99
		Martis et al. [46]	EMD + spectral features	95.3	98.0	97.0
		Orhan et al. [62]	DWT + K-means clustering + MLPNN	96.7	94.1	99.0
		Hassan et al. [63]	CEEMDAN + NIG	98.7	98.7	98.7
	S-F-Z	Present work	EMD	97.7	96.4	98.4
			EEMD	98.6	96.0	99.9
			CEEMDAN	98.5	97.8	99.4
			EWT	97.1	95.9	97.7
			VMD	98.3	97.9	98.6
			Original signal	95.1	93.0	96.2
	XY-Z	Gupta et al. [58]	DCT + Hurst Exponent + ARMA Parameters	89.3	91.8	94.30
		Gupta et al. [58]	DCT + Hurst Exponent + ARMA Parameters	96.5	97.2	95.8
NSC-ND	Y-Z	Swami et al. [64]	DT-CWT	97.3	99.0	99.9
		Swami et al. [65]	DT-CWT + GRNN	98.1	99.4	99.7
		Gandhi et al. [36]	DWT + PNN + DHS_MD	100	100	100
		Present work	EMD	99.0	98.0	100
			EEMD	100	100	100
			CEEMDAN	98.4	96.8	100
			EWT	100	100	100
			VMD	100	100	100
			Original signal	98.1	96.6	99.6

4. Discussion

Best-case results are similar among all five decomposition methods, with slight superior values for EEMD, CEEMDAN and VMD. Furthermore, disparate performances were not observed when comparing different classifiers. This might reflect an overall good feature extraction quality obtained by the evaluated adaptive decomposition methods. Results for original non-decomposed signals were inferior, with the exception of the time-consuming GPC classifier, which achieved a fairly high accuracy of 95.1% for UoB dataset and 98.1% (Y-Z) or 96.7% (X-Y-Z) for NSC-ND. Thus, the burden falls on the classifier when the set of features is extracted

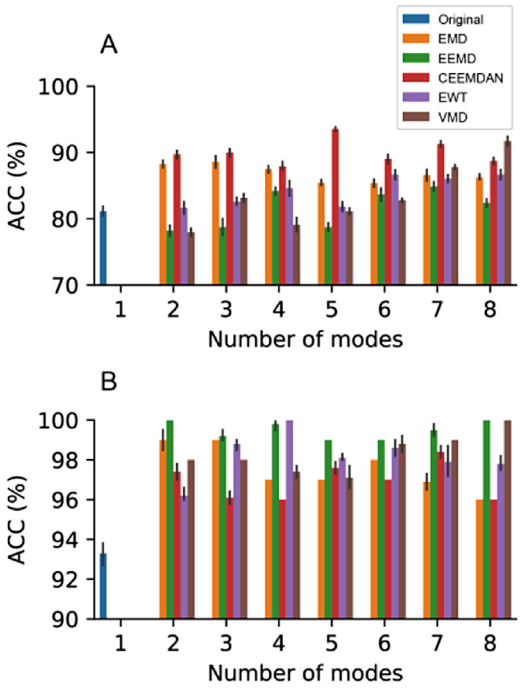

Fig. 9. Accuracy values as a function of decomposed modes. RBF-SVM accuracy values are shown for features extracted from the original signal and from the analysed decomposition methods, varying the number of modes. (A) Sets X-Y-Z (pre-ictal x inter-ictal x ictal) and (B) Y-Z (inter-ictal x ictal) of the NSC-ND dataset.

from the original signal, while the adaptive decomposition methods evaluated in this work provide better class separability. This would have implications for implementing any of these methods on automated seizure detection devices, where the tradeoff between computational power and performance is critical. That is, the gain in prediction power should be weighed against the additional execution time required by a decomposition algorithm and classifier when developing an automated real-time seizure detection system.

Performance values are in accordance with the literature, which has classification accuracies varying from 90% in Ref. [66] to 99.4 % in Ref. [59] for the UoB dataset and around 89 % for NSC-ND [58]. When considering normal x ictal classes, some works achieve 100 % ACC [36,63] Works using other datasets also achieve 100% performances for automated seizure detection [20].

Although specific tuning of classifier parameters for each method could increase performances, the same default parameters were chosen for all decomposition methods. This was done considering the main goal of this work, which is not to propose a new seizure detection method, but to evaluate and compare decomposition methods under the same conditions. That is, given the same classifiers applied to the same set of spectral and time-domain features, what is the impact of using different adaptive decomposition methods on classification performance? We found that these methods provide better class separability in relation to the non-decomposed signal and rather similar best-case performances among them. Furthermore, the number of iterations to reach the optimum number of modes varies according to the decomposition method and dataset, such that this parameter should be carefully chosen in order to maximize the potential of each decomposition method – e.g. while VMD reached best ACC with eight modes, EMD performed better with only two IMFs (using the NSC-ND dataset).

The methods evaluated in this work aim to adaptively decompose a signal into AM-FM components and extract features of each mode, in order to differentiate normal and seizure-free signals from seizure ones. This has promising applications for the identification of epileptogenic systems and for identifying interictal to ictal state transitions. The feature extraction capabilities can be further explored if each mode was considered as having "well behaved" Hilbert Transforms, which enables the analysis of phase relationships between different modes of the same signal or between different brain regions, if multichannel data is available. Since synchronization is believed to play an important role for ictogenesis, these methods may further assist in unveiling the mechanisms of seizure generation and devising markers to predict transitions to ictal states.

Interpretation of the results must consider the limitations of the used benchmark EEG datasets. While these are very useful for algorithm evaluation and comparison with similar works, the data on both consists of selected short segments obtained in relatively controlled conditions. Thus, these have light requirements in terms of generalization and robustness to artifacts and changes in brain states when compared with what would be found in a clinical environment. Thus, it is likely that greater discrepancies should be observed between the analyzed decomposition methods in this work if these were applied in a clinical setting or in embedded devices. Nevertheless, the use of such benchmark datasets is an important and necessary evaluation step that should be considered for all seizure detection and prediction methods.

5. Conclusion

The development of feature extraction and classification methods is a key step both for understanding of the operating mechanisms of epilepsy, as for clinical analysis, including possible applications for seizure detection and prediction devices.

This work has shown that best-case seizure detection results are similar among the evaluated adaptive decomposition methods but the number of extracted modes should be adjusted according to the decomposition method and data at hand in order to reach optimal performances. Slightly superior values were found for VMD, EEMD and CEEMDAN. However, the extended versions of EMD also resulted in greater execution times, which may hamper the use of such methods in real-time applications. Good tradeoffs between computational cost and performance could be found with VMD and EWT, which was the fastest decomposition method.

The use of adaptive decomposition methods is a promising approach due to their ability to separate different AM-FM components that are altered in the presence of seizures (and possibly on periods preceding these events). This would facilitate the extraction of features related to these events, increasing the performance of classification algorithms. However, the extraction of the same features from non-decomposed signal still results in fairly accurate classifiers. Thus, in contexts with the need of real time processing and limited computational power, the performance gains should be weighed against the additional required computational cost of such decomposition algorithms.

Another goal of this work was to provide a Python code of these signal decomposition methods for the community. Python is a fast-growing programming language and is currently the third most popular programming language in the world [67] and with widespread applications in neuroscience [68]. The distribution of these packages could further encourage the use of open source programming languages for works involving these specific signal processing methods.

Declarations of interest

The authors report no declarations of interest.

CRediT authorship contribution statement

Vinícius R. Carvalho: Conceptualization, Methodology, Software, Validation, Data curation, Writing - original draft, Writing - review & editing, Visualization. **Márcio F.D. Moraes:** Resources, Supervision, Writing - review & editing, Funding acquisition. **Antônio P. Braga:** Conceptualization, Writing - review & editing. **Eduardo M.A.M. Mendes:** Conceptualization, Writing - review & editing, Supervision.

Appendix A. Supplementary data

Supplementary material related to this article can be found, in the online version, at doi:https://doi.org/10.1016/j.bspc.2020.102073.

References

[1] K.M. Fiest, K.M. Sauro, S. Wiebe, S.B. Patten, C.-S. Kwon, J. Dykeman, T. Pringsheim, D.L. Lorenzetti, N. Jetté, Prevalence and incidence of epilepsy, Neurology 88 (2017) 296–303, http://dx.doi.org/10.1212/WNL.0000000000003509.

[2] L. Sander, The epidemiology of the Epilepsies revisited, Curr. Opin. Neurol. 16 (2003) 165–170, http://dx.doi.org/10.1097/01.wco.0000063766.15877.8e.

[3] R.S. Fisher, C. Acevedo, A. Arzimanoglou, A. Bogacz, J.H. Cross, C.E. Elger, J. Engel, L. Forsgren, J.A. French, M. Glynn, D.C. Hesdorffer, B.I. Lee, G.W. Mathern, S.L. Moshé, E. Perucca, I.E. Scheffer, T. Tomson, M. Watanabe, S. Wiebe, ILAE official report: a practical clinical definition of epilepsy, Epilepsia 55 (2014) 475–482, http://dx.doi.org/10.1111/epi.12550.

[4] J. Engel, T. Pedley, Epilepsy – A Comprehensive Textbook, 1989, http://dx.doi.org/10.1017/CBO9781107415324.004.

[5] F.H. Lopes da Silva, The impact of EEG/MEG signal processing and modeling in the diagnostic and management of Epilepsy, IEEE Rev. Biomed. Eng. 1 (2008) 143–156, http://dx.doi.org/10.1109/RBME.2008.2008246.

[6] H. Adeli, Z. Zhou, N. Dadmehr, Analysis of EEG records in an epileptic patient using wavelet transform, J. Neurosci. Methods. 123 (2003) 69–87 http://www.ncbi.nlm.nih.gov/pubmed/12581851.

[7] U.R. Acharya, S. Vinitha Sree, G. Swapna, R.J. Martis, J.S. Suri, Automated EEG analysis of epilepsy: a review, Knowledge-Based Syst. 45 (2013) 147–165, http://dx.doi.org/10.1016/j.knosys.2013.02.014.

[8] S. Ramgopal, S. Thome-Souza, M. Jackson, N.E. Kadish, I. Sánchez Fernández, J. Klehm, W. Bosl, C. Reinsberger, S. Schachter, T. Loddenkemper, Seizure detection, seizure prediction, and closed-loop warning systems in epilepsy, Epilepsy Behav. 37 (2014) 291–307, http://dx.doi.org/10.1016/j.yebeh.2014.06.023.

[9] F. Mormann, R.G. Andrzejak, C.E. Elger, K. Lehnertz, Seizure prediction: the long and winding road, Brain 130 (2007) 314–333, http://dx.doi.org/10.1093/brain/awl241.

[10] N.E. Huang, Z. Shen, S.R. Long, M.C. Wu, H.H. Shih, Q. Zheng, N.-C. Yen, C.C. Tung, H.H. Liu, The empirical mode decomposition and the Hilbert spectrum for nonlinear and non-stationary time series analysis, Proc. R. Soc. A Math. Phys. Eng. Sci. 454 (1998) 903–995, http://dx.doi.org/10.1098/rspa.1998.0193.

[11] R.B. Pachori, Discrimination between Ictal and Seizure-Free EEG signals using empirical mode decomposition, Res. Lett. Commun. 2008 (2008) 1–5, http://dx.doi.org/10.1155/2008/293056.

[12] G. Rilling, P. Flandrin, P. Goncalves, J.M. Lilly, Bivariate empirical mode decomposition, IEEE Signal Process. Lett. 14 (2007) 936–939, http://dx.doi.org/10.1109/LSP.2007.904710.

[13] N. Rehman, D.P. Mandic, Multivariate empirical mode decomposition, Proc. R. Soc. A Math. Phys. Eng. Sci. 466 (2010) 1291–1302, http://dx.doi.org/10.1098/rspa.2009.0502.

[14] M.E. Torres, M.A. Colominas, G. Schlotthauer, P. Flandrin, A complete ensemble empirical mode decomposition with adaptive noise, 2011 IEEE Int. Conf. Acoust. Speech Signal Process., IEEE (2011) 4144–4147, http://dx.doi.org/10.1109/ICASSP.2011.5947265.

[15] Z. Wu, N.E. Huang, Ensemble empirical mode decomposition: a noise-assisted data analysis method, Adv. Adapt. Data Anal. 1 (2009) 1–41, http://dx.doi.org/10.1142/S1793536909000047.

[16] C.M. Sweeney-Reed, S.J. Nasuto, M.F. Vieira, A.O. Andrade, Empirical mode decomposition and its extensions applied to EEG analysis: a review, Adv. Data Sci. Adapt. Anal. 10 (2018) 1840001, http://dx.doi.org/10.1142/s2424922x18400016.

[17] A. Zahra, N. Kanwal, N. ur Rehman, S. Ehsan, K.D. McDonald-Maier, Seizure detection from EEG signals using multivariate empirical mode decomposition, Comput. Biol. Med. 88 (2017) 132–141, http://dx.doi.org/10.1016/j.compbiomed.2017.07.010.

[18] R.J. Oweis, E.W. Abdulhay, Seizure classification in EEG signals utilizing Hilbert-Huang transform, Biomed. Eng. Online 10 (2011) 38 (Accessed 12 November 2013) http://www.biomedical-engineering-online.com/content/10/1/38.

[19] V. Bajaj, R. Pachori, Classification of seizure and non-seizure EEG signals using Empirical Mode Decomposition, IEEE J. Biomed. Heal. Informatics. 16 (2011) 1135–1142, http://dx.doi.org/10.1109/TITB.2011.2181403.

[20] E. Alickovic, J. Kevric, A. Subasi, Performance evaluation of empirical mode decomposition, discrete wavelet transform, and wavelet packed decomposition for automated epileptic seizure detection and prediction, Biomed. Signal Process. Control. 39 (2018) 94–102, http://dx.doi.org/10.1016/j.bspc.2017.07.022.

[21] S. Li, W. Zhou, Q. Yuan, S. Geng, D. Cai, Feature extraction and recognition of ictal EEG using EMD and SVM, Comput. Biol. Med. 43 (2013) 807–816, http://dx.doi.org/10.1016/j.compbiomed.2013.04.002.

[22] J. Gilles, Empirical wavelet transform, IEEE Trans. Signal Process. 61 (2013) 3999–4010, http://dx.doi.org/10.1109/TSP.2013.2265222.

[23] R. Kumar, I. Saini, Empirical wavelet transform based ECG signal compression, IETE J. Res. 60 (2014) 423–431, http://dx.doi.org/10.1080/03772063.2014.963173.

[24] W. Liu, S. Cao, Y. Chen, Seismic time-frequency analysis via empirical wavelet transform, IEEE Geosci. Remote Sens. Lett. 13 (2016) 28–32, http://dx.doi.org/10.1109/LGRS.2015.2493198.

[25] A. Bhattacharyya, L. Singh, R.B. Pachori, Fourier–bessel series expansion based empirical wavelet transform for analysis of non-stationary signals, Digit. Signal Process. A Rev. J. 78 (2018) 185–196, http://dx.doi.org/10.1016/j.dsp.2018.02.020.

[26] J. Gabor, R.R. Leach, F.U. Dowla, Automated seizure detection using a self-organizing neural network, Electroencephalogr. Clin. Neurophysiol. 99 (1996) 257–266 http://www.ncbi.nlm.nih.gov/pubmed/22824647.

[27] H. Bahcivan, N. Zhang, Cross-correlation analysis of epileptiform propagation using wavelets, Med (2001) 1804–1807 (Accessed 8 April 2014) http://ieeexplore.ieee.org/xpls/abs_all.jsp?arnumber=1020571.

[28] D. Chen, S. Wan, J. Xiang, F.S. Bao, A high-performance seizure detection algorithm based on Discrete Wavelet Transform (DWT) and EEG, PLoS One 12 (2017) 1–21, http://dx.doi.org/10.1371/journal.pone.0173138.

[29] A. Bhattacharyya, M. Sharma, R.B. Pachori, P. Sircar, U.R. Acharya, A novel approach for automated detection of focal EEG signals using empirical wavelet transform, Neural Comput. Appl. 29 (2018) 47–57, http://dx.doi.org/10.1007/s00521-016-2646-4.

[30] S. Saxena, C. Hemanth, R.G. Sangeetha, Classification of normal, seizure and seizure-free EEG signals using EMD and EWT, 2017 Int. Conf. Nextgen Electron. Technol. Silicon to Softw., IEEE (2017) 360–366, http://dx.doi.org/10.1109/ICNETS2.2017.8067961.

[31] K. Dragomiretskiy, D. Zosso, Variational mode decomposition, IEEE Trans. Signal Process. 62 (2014) 531–544, http://dx.doi.org/10.1109/TSP.2013.2288675.

[32] M. Ravi Kumar, Y. Srinivasa Rao, Epileptic seizures classification in EEG signal based on semantic features and variational mode decomposition, Cluster Comput. 4 (2018) 1–11, http://dx.doi.org/10.1007/s10586-018-1995-4.

[33] T. Zhang, W. Chen, M. Li, AR based quadratic feature extraction in the VMD domain for the automated seizure detection of EEG using random forest classifier, Biomed. Signal Process. Control. 31 (2017) 550–559, http://dx.doi.org/10.1016/j.bspc.2016.10.001.

[34] S. Taran, V. Bajaj, Clustering variational mode decomposition for identification of focal EEG signals, IEEE Sensors Lett. 2 (2018) 1–4, http://dx.doi.org/10.1109/LSENS.2018.2872415.

[35] R. Andrzejak, K. Lehnertz, F. Mormann, C. Rieke, P. David, C. Elger, Indications of nonlinear deterministic and finite-dimensional structures in time series of brain electrical activity: dependence on recording region and brain state, Phys. Rev. E. 64 (2001), 061907, http://dx.doi.org/10.1103/PhysRevE.64.061907.

[36] T.K. Gandhi, P. Chakraborty, G.G. Roy, B.K. Panigrahi, Discrete harmony search based expert model for epileptic seizure detection in electroencephalography, Expert Syst. Appl. 39 (2012) 4055–4062, http://dx.doi.org/10.1016/j.eswa.2011.09.093.

[37] P. Swami, T.K. Gandhi, B.K. Panigrahi, M. Tripathi, S. Anand, A novel robust diagnostic model to detect seizures in electroencephalography, Expert Syst. Appl. 56 (2016) 116–130, http://dx.doi.org/10.1016/j.eswa.2016.02.040.

[38] P. Swami, B.K. Panigrahi, S. Nara, M. Bhatia, T.K. Gandhi, EEG Epilepsy Datasets, 2016, http://dx.doi.org/10.13140/RG.2.2.14280.32006.

[39] M.A. Colominas, G. Schlotthauer, M.E. Torres, Improved complete ensemble EMD: a suitable tool for biomedical signal processing, Biomed. Signal Process. Control. 14 (2014) 19–29, http://dx.doi.org/10.1016/j.bspc.2014.06.009.

[40] D. Laszuk, Python Implementation of Empirical Mode Decomposition Algorithm, 2017 https://laszukdawid.com/codes/.

[41] I. Daubechies, Ten Lectures on Wavelets, Society for Industrial and Applied Mathematics, 1992, http://dx.doi.org/10.1137/1.9781611970104.

[42] J. Gilles, Empirical Wavelet Transforms, (n.d.). https://www.mathworks.com/matlabcentral/fileexchange/42141-empirical-wavelet-transforms.

[43] R.T. Rockafellar, A dual approach to solving nonlinear programming problems by unconstrained optimization, Math. Program. 5 (1973) 354–373, http://dx.doi.org/10.1007/BF01580138.

[44] M.R. Hestenes, Multiplier and gradient methods, J. Optim. Theory Appl. 4 (1969) 303–320, http://dx.doi.org/10.1007/BF00927673.

[45] D. Zosso, Variational Mode Decomposition Toolbox, 2013 https://www.mathworks.com/matlabcentral/fileexchange/44765-variational-mode-decomposition.

[46] R.J. Martis, U.R. Acharya, J.H. Tan, A. Petznick, R. Yanti, C.K. Chua, E.Y.K. Ng, L. Tong, Application of empirical mode decomposition (emd) for automated

detection of epilepsy using EEG signals, Int. J. Neural Syst. 22 (2012) 1250027, http://dx.doi.org/10.1142/S012906571250027X.
[47] P. Welch, The use of fast Fourier transform for the estimation of power spectra: a method based on time averaging over short, modified periodograms, IEEE Trans. Audio Electroacoust. 15 (1967) 70–73, http://dx.doi.org/10.1109/TAU.1967.1161901.
[48] L. Cohen, C. Lee, Instantaneous bandwidth for signals and spectrogram, Int. Conf. Acoust. Speech, Signal Process. (1990) 2451–2454, http://dx.doi.org/10.1109/ICASSP.1990.116086.
[49] B. Hjorth, EEG analysis based on time domain properties, Electroencephalogr. Clin. Neurophysiol. 29 (1970) 306–310 (Accessed 9 October 2016) http://www.ncbi.nlm.nih.gov/pubmed/4195653.
[50] M.A. Navascués, M.V. Sebastián, Time domain indices and discrete power spectrum in electroencephalographic processing, Int. J. Comput. Math. 86 (2009) 1968–1978, http://dx.doi.org/10.1080/00207160903023599.
[51] F. Pedregosa, G. Varoquaux, A. Gramfort, V. Michel, B. Thirion, O. Grisel, M. Blondel, A. Müller, J. Nothman, G. Louppe, P. Prettenhofer, R. Weiss, V. Dubourg, J. Vanderplas, A. Passos, D. Cournapeau, M. Brucher, M. Perrot, É. Duchesnay, Scikit-learn: machine learning in python, J. Mach. Learn. Res. 12 (2012) 2825–2830 https://dl.acm.org/citation.cfm?id=2078195.
[52] I. Guyon, J. Weston, S. Barnhill, V. Vapnik, Gene selection for cancer classification using support vector machines, Mach. Learn. 46 (2002) 389–422, http://dx.doi.org/10.1023/A:1012487302797.
[53] N.S. Altman, An introduction to kernel and nearest-neighbor nonparametric regression, Am. Stat. 46 (1992) 175–185, http://dx.doi.org/10.1080/00031305.1992.10475879.
[54] C. Cortes, V. Vapnik, Support-vector networks, Mach. Learn. 20 (1995) 273–297, http://dx.doi.org/10.1007/BF00994018.
[55] C.E. Rasmussen, C.K.I. Williams, Gaussian Processes for Machine Learning, The MIT Press, Cambridge, Massachusetts, 2006, http://dx.doi.org/10.1142/S0129065704001899.
[56] G.E. Hinton, Connectionist learning procedures, Artif. Intell. 40 (1989) 185–234, http://dx.doi.org/10.1016/0004-3702(89)90049-0.
[57] R. Sharma, R.B. Pachori, P. Sircar, Seizures classification based on higher order statistics and deep neural network, Biomed. Signal Process. Control. 59 (2020) 101921, http://dx.doi.org/10.1016/j.bspc.2020.101921.
[58] A. Gupta, P. Singh, M. Karlekar, A novel signal modeling approach for classification of seizure and seizure-free EEG signals, IEEE Trans. Neural Syst. Rehabil. Eng. 26 (2018) 925–935, http://dx.doi.org/10.1109/TNSRE.2018.2818123.
[59] A. Subasi, J. Kevric, M. Abdullah Canbaz, Epileptic seizure detection using hybrid machine learning methods, Neural Comput. Appl. 31 (2019) 317–325, http://dx.doi.org/10.1007/s00521-017-3003-y.
[60] U.R. Acharya, S.L. Oh, Y. Hagiwara, J.H. Tan, H. Adeli, Deep convolutional neural network for the automated detection and diagnosis of seizure using EEG signals, Comput. Biol. Med. 100 (2018) 270–278, http://dx.doi.org/10.1016/j.compbiomed.2017.09.017.
[61] U. Rajendra Acharya, S. Vinitha Sree, A.P.C. Alvin, J.S. Suri, Use of principal component analysis for automatic classification of epileptic EEG activities in wavelet framework, Expert Syst. Appl. 39 (2012) 9072–9078, http://dx.doi.org/10.1016/j.eswa.2012.02.040.
[62] U. Orhan, M. Hekim, M. Ozer, EEG signals classification using the K-means clustering and a multilayer perceptron neural network model, Expert Syst. Appl. 38 (2011) 13475–13481, http://dx.doi.org/10.1016/j.eswa.2011.04.149.
[63] A.R. Hassan, A. Subasi, Y. Zhang, Epilepsy seizure detection using complete ensemble empirical mode decomposition with adaptive noise, Knowledge-Based Syst. 191 (2020), http://dx.doi.org/10.1016/j.knosys.2019.105333.
[64] P. Swami, T.K. Gandhi, B.K. Panigrahi, M. Bhatia, J. Santhosh, S. Anand, A comparative account of modelling seizure detection system using wavelet techniques, Int. J. Syst. Sci. Oper. Logist. 4 (2017) 41–52, http://dx.doi.org/10.1080/23302674.2015.1116637.
[65] P. Swami, M. Bhatia, M. Tripathi, P.S. Chandra, B.K. Panigrahi, T.K. Gandhi, Selection of optimum frequency bands for detection of epileptiform patterns, Healthc. Technol. Lett. 6 (2019) 126–131, http://dx.doi.org/10.1049/htl.2018.5051.
[66] K.C. Hsu, S.N. Yu, Detection of seizures in EEG using subband nonlinear parameters and genetic algorithm, Comput. Biol. Med. 40 (2010) 823–830, http://dx.doi.org/10.1016/j.compbiomed.2010.08.005.
[67] The State of the Octoverse, 2018 https://octoverse.github.com/.
[68] E. Muller, J.A. Bednar, M. Diesmann, M.-O. Gewaltig, M. Hines, A.P. Davison, Python in neuroscience, Front. Neuroinform. 9 (2015) 14–17, http://dx.doi.org/10.3389/fninf.2015.00011.